J|A|C|S ARTICLES

Published on Web 02/25/2010

Crystal Transformation and Host Molecular Motions in CO_2 Adsorption Process of a Metal Benzoate Pyrazine (M^{II} = Rh, Cu)

Satoshi Takamizawa,*[,†,‡] Ei-ichi Nataka,[†] Takamasa Akatsuka,[†] Ryosuke Miyake,[†] Yoshiki Kakizaki,[§] Hirotoshi Takeuchi,[§] Goro Maruta,[§] and Sadamu Takeda[§]

Department of Nanosystem Science, Graduate School of Nanobioscience, Yokohama City University, 22-2 Seto, Kanazawa-ku, Yokohama 236-0027, Japan, PRESTO, Japan Science and Technology Agency (JST), Honcho, Kawaguchi, Saitama 332-0012, Japan, and Department of Chemistry, Faculty of Science and Graduate School of Science, Hokkaido University, Sapporo 060-0810, Japan

Received October 28, 2009; E-mail: staka@yokohama-cu.ac.jp

Abstract: For the purpose of investigating the correlation between host gas adsorption ability and structural flexibility, the combination of metal benzoate complexes $[M^{II}_2(bza)_4]$ (M^{II} = Rh (**a**), Cu (**b**); bza = benzoate) and pyrazine derivatives (pyz = pyrazine (**1**), 2-mpyz = 2-methylpyrazine (**2**), 2,3-dmpyz = 2,3-dimethylpyrazine (**3**)) yields a series of one-dimensionally assembled complexes. The study of the adsorption properties of this series was examined for CO_2, H_2, N_2, O_2, and Ar gases at 195 K (CO_2) or at 77 K (all others). The adsorption manners of these complexes are similar for each gas, while the pressure at which adsorption started or rapidly grew increased with a rise in the number of methyl groups in the case of adsorbable gases. The maximum amount of adsorption was a positive integer, e.g., 3 molecules per M_2 unit for **1** and **2** and 2 molecules per M_2 unit for **3** in the case of CO_2 adsorption for all complexes at 0.1 MPa of adsorbable gases. Structural transformation was observed accompanying gas adsorption. This transformation was observed when the adsorption amount reached 1 molecule per M_2 unit, suggesting a correlation of the adsorption amount and dynamic adsorption behavior. Single-crystal X-ray analyses of nonincluded crystals and CO_2 inclusions for all hosts (**1**−**3**) revealed that large structural changes occurred through CO_2 adsorption to increase the inner space for adsorption gases, depending on the substituents on the pyrazine ring. These facts were confirmed as a transition by DSC measurements using a mixed CO_2/N_2 gas atmosphere. Solid-state ^{1}H and ^{2}H NMR studies of the crystalline sample of **1a** and its partially deuterated samples of **1a′** (deuterated phenyl group) and **1a″** (deuterated pyrazine) revealed rapid 180°-flip motions of the aromatic rings of the host skeletons, which form the walls of the channels. These "rotating" motions would help the diffusion of CO_2 molecules through a narrow channel at relatively low pressure. Indeed, the motions of phenyl groups and methyl-substituted pyrazine moieties of phenyl deuterated **3a** were confirmed to be very slow by solid-state ^{1}H and ^{2}H NMR spectra, where the amount of adsorbed gas molecules was small for **3a** at 0.1 MPa of CO_2.

Introduction

Metal−organic porous materials have been widely investigated as a new class of materials following the well-known activated carbon and zeolites.[1] These materials possess ordered cavities and channels that are easy to rationally design and control, which would allow selective adsorption applicable to sensor and separation techniques.[2] In particular, flexible frameworks based on weak interactions such as the coordination bond, $\pi-\pi$ stacking, and van der Waals contact can demonstrate large structural changes with retained crystallinity during the adsorption process.[3] As compared with conventional adsorbents, this dynamic change in the host skeleton might pave the way for a promising system of novel separation techniques and of probes

[†] Yokohama City University.
[‡] PRESTO.
[§] Hokkaido University.

(1) (a) Yaghi, O. M.; O'Keeffe, M.; Ockwig, N. W.; Chae, H. K.; Eddaoudi, M.; Kim, J. *Nature* **2003**, *423*, 705. (b) Kitagawa, S.; Kitaura, R.; Noro, S. *Angew. Chem., Int. Ed.* **2004**, *43*, 2334. (c) Férey, G.; Mellot-Draznieks, C.; Serre, C.; Millange, F. *Acc. Chem. Res.* **2005**, *38*, 217. (d) Bradshaw, D.; Claridge, J. B.; Cussen, E. J.; Prior, T. J.; Rosseinsky, M. J. *Acc. Chem. Res.* **2005**, *38*, 273. (e) Mori, W.; Takamizawa, S. in *Organometallic Conjugation*; Nakamura, A., Ueyama, N., Yamaguchi, K., Eds.; Springer: Tokyo, 2002; Chapter 6, pp 179−213.

(2) For example:(a) Kondo, A.; Noguchi, H.; Carlucci, L.; Proserpio, D. M.; Ciani, G.; Kajiro, H.; Ohba, T.; Kanoh, H.; Kaneko, K. *J. Am. Chem. Soc.* **2007**, *129*, 12362. (b) Dybtsev, D. N.; Chun, H.; Yoon, S. H.; Kim, D.; Kim, K. *J. Am. Chem. Soc.* **2004**, *126*, 32. (c) Shimomura, S.; Matsuda, R.; Tsujino, T.; Kawamura, T.; Kitagawa, S. *J. Am. Chem. Soc.* **2006**, *128*, 16416. (d) Maji, T. K.; Uemura, K.; Chang, H.-C.; Matsuda, R.; Kitagawa, S. *Angew. Chem., Int. Ed.* **2004**, *43*, 3269. (e) Atwood, J. L.; Barbour, L. J.; Jerga, A. *Angew. Chem., Int. Ed.* **2004**, *43*, 2948. (f) Matsuda, R.; Kitaura, R.; Kitagawa, S.; Kubota, Y.; Belosludov, R. V.; Kobayashi, T. C.; Sakamoto, H.; Chiba, T.; Takata, M.; Kawazoe, Y.; Mita, Y. *Nature* **2005**, *436*, 238. (g) Pan, L.; Olson, D. H.; Ciemnolonski, L. R.; Heddy, R.; Li, J. *Angew. Chem., Int. Ed.* **2006**, *45*, 616. (h) Chen, B.; Liang, C.; Yang, J.; Contreras, D. S.; Clancy, Y. L.; Lobkovsky, E. B.; Yaghi, O. M.; Dai, S. *Angew. Chem., Int. Ed.* **2006**, *45*, 1390. (i) Chong, J. H.; MacLachlan, M. J. *Inorg. Chem.* **2006**, *45*, 1442. (j) Fairchild, R. M.; Holman, K. T. *J. Am. Chem. Soc.* **2005**, *127*, 16364. (k) Alaerts, L.; Maes, M.; Giebeler, L.; Jacobs, P. A.; Martens, J. A.; Denayer, J. F. M.; Kirschhock, C. E. A.; De Vos, D. E. *J. Am. Chem. Soc.* **2008**, *130*, 14170. (l) Takamizawa, S.; Kohbara, M.; Miyake, R. *Chem. Asian J.* **2009**, *4*, 530. (m) Takamizawa, S.; Miyake, R. *Chem. Commun.* **2009**, 4076.

for detection of specific molecules from a gas mixture. Single-crystal adsorbents should contribute to the investigation of the mechanism of adsorption through observation of these aggregate structures because their high degree of integrity and regularity can control guest alignment.[4] Since materials for which the structure is well understood allow a microscopic view of the relationship between structure and physical properties, the study of structure concerning thermal properties is important to understand functional materials.[5] Recently, we reported the single-crystal adsorbents $[M^{II}_2(bza)_4(pyz)]_n$ (M^{II} = Rh (**1a**), Cu (**1b**); bza = benzoate; pyz = pyrazine) and their derivatives as good candidates for such observations.[6−8] Molecular crystals formed by van der Waals interaction exhibit high flexibility and adjustability for the properties of adsorbed guests. Because the crystallinity is maintained after the adsorption process, this series enabled us to determine the structures at the gas inclusion state by single-crystal crystallography and their dynamics in solid state. Since the study of molecular motion coupled with adsorption phenomena is an important issue for revealing the invasion and diffusion mechanisms of guests through the channel,[9] a systematic study of adsorption processes accompanied by structural change is required.

In this article, we report the preparation of a series of single-crystal adsorbents $[M^{II}_2(bza)_4(Rpyz)]_n$ (M^{II} = Rh (**a**), Cu (**b**); R = H (**1**), 2-methyl (**2**), 2,3-dimethyl (**3**)) (Chart 1). Methyl groups were introduced in the channels of **2** and **3**. Since CO_2 gas adsorption induces clear structural transition for the hosts under moderate conditions,[7] systematic study of CO_2 gas adsorption of the host series is appropriate for clarifying the correlation between the structures and the dynamic adsorption behaviors. In order to prove the change in local dynamic motion of a host lattice induced by CO_2 gas and by methyl substitution of the pyrazine moiety, solid-state ^2H NMR measurements of deuterated compounds of **1a**−**3a** were performed. In addition to this function, clarification of the adsorption mechanism of CO_2 gas on porous materials will also be important since CO_2 gas is widely known to contribute to the greenhouse effect.

Chart 1. Infinite Chain Structure of Compounds **1**−**3**

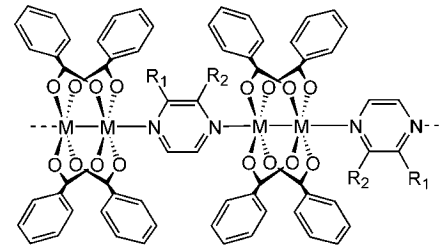

$[M^{II}_2(bza)_4(Rpyz)]_n$

$R_1 = R_2 = H$ (**1**) M = Rh^{II} (**a**), Cu^{II} (**b**)

$R_1 = H$, $R_2 = Me$ (**2**)

$R_1 = R_2 = Me$ (**3**)

Results and Discussion

Preparation of Single-Crystal Host Family. To extend a series of the single-crystal hosts $[M_2(bza)_4(pyz)]_n$ possessing a flexible 1D channel in which various gaseous molecules are encapsulated, single-crystal hosts $[M^{II}_2(bza)_4(Rpyz)]_n$ (M^{II} = Rh (**a**), Cu (**b**); R = H (**1**), 2-methyl (**2**), 2,3-dimethyl (**3**)) were synthesized (Chart 1). These compounds consist of a 1:1 assembly of a pyrazine derivative and a lantern-type metal complex[10] $[M^{II}_2(bza)_4]$. The structures of the single-crystal hosts were determined by single-crystal X-ray analysis (Table 1 and Tables S1–2); it appeared that the channel (diameter: ∼2−4 Å) runs regularly in all of the crystals (Figure S1, Supporting Information).

In contrast to **1**,[7,8] possessing a straight one-dimensional (1-D) chain structure, newly synthesized complexes **2b**, **3a**, and **3b** possess an infinite zigzag 1-D chain structure similar to that in **2a**,[11] which is caused by the steric hindrance of methyl groups introduced in the pyrazine ring (refer to Figures 6a and 7a for Rh complexes). The additional methyl groups reduced the void volume at 298 K, which is a indicator of the channel spaces, by 19, 9, 39, and 44% for **2a**, **2b**, **3a**, and **3b**, respectively, as compared with that observed in **1a** and **1b**. The crystals of **3** show even more bent chain structures than do those in **2**. This is attributed to a greater steric hindrance due to two methyl groups (M−pyz(center)−M angles at 298 K: 169.78°, 169.77°, 164.84°, 164.34°, (at 90 K: 169.74°, 169.88°, 164.91°, 164.29°) for **2a**, **2b**, **3a**, and **3b**, respectively). These zigzag chains were stacked on each other through phenyl−phenyl and phenyl−pyrazine interactions, which generate void spaces. This packing feature is similar to those observed in crystals of **1a** and **1b**.

(3) (a) Cussen, E. J.; Claridge, J. B.; Rosseinsky, M. J.; Kepert, C. J. *J. Am. Chem. Soc.* **2002**, *124*, 9574. (b) Côté, A. P.; Ferguson, M. J.; Khan, K. A.; Enright, G. D.; Kulynych, A. D.; Dalrymple, S. A.; Shimizu, G. K. H. *Inorg. Chem.* **2002**, *41*, 287. (c) Kitagawa, S.; Uemura, K. *Chem. Soc. Rev.* **2005**, *34*, 109. (d) Fletcher, A. J.; Thomas, Rosseinsky, M. J. *J. Solid State Chem.* **2005**, *178*, 2491. (e) Llewellyn, P. L.; Bourrelly, S.; Serre, C.; Filinchuk, Y.; Férey, G. *Angew. Chem., Int. Ed.* **2006**, *46*, 7751. (f) Ghosh, S. K.; Bureekaew, S.; Kitagawa, S. *Angew. Chem., Int. Ed.* **2008**, *47*, 3403. (g) Millange, F.; Serre, C.; Guillou, N.; Férey, G.; Walton, R. I. *Angew. Chem., Int. Ed.* **2008**, *47*, 4100. (h) Tanaka, D.; Nakagawa, K.; Higuchi, M.; Horike, S.; Kubota, Y.; Kobayashi, T. C.; Tanaka, M.; Kitagawa, S. *Angew. Chem., Int. Ed.* **2008**, *47*, 3914. (i) Chandler, B. D.; Enright, G. D.; Udachin, K. A.; Pawsey, Shane; Ripmeester, J. A.; Cramb, D. T.; Shimizu, G. K. *Nat. Mater.* **2008**, *7*, 229. (j) Seo, J.; Matsuda, R.; Sakamoto, H.; Bonneau, C.; Kitagawa, S. *J. Am. Chem. Soc.* **2009**, *131*, 12793.

(4) (a) Braga, D.; Curzi, M.; Johansson, A.; Polito, M.; Rubini, K.; Grepioni, F. *Angew. Chem., Int. Ed.* **2006**, *45*, 142. (b) Lee, E. Y.; Suh, M. P. *Angew. Chem., Int. Ed.* **2004**, *43*, 2798. (c) Takaoka, K.; Kawano, M.; Tominaga, M.; Fujita, M. *Angew. Chem., Int. Ed.* **2005**, *44*, 2151. (d) Halder, G. J.; Kepert, C. J. *J. Am. Chem. Soc.* **2005**, *127*, 17152. (e) Spencer, E. C.; Howard, A. K.; McIntyre, G. J.; Rowsell, L. C.; Yaghi, O. M. *Chem. Commun.* **2006**, 278. (f) Papaefstathiou, G. S.; Friščić, T.; MacGillivray, L. R. *J. Am. Chem. Soc.* **2005**, *127*, 14160. (g) Sumby, C. J.; Hardie, M. J. *Angew. Chem., Int. Ed.* **2005**, *44*, 6395. (h) Thallapally, P. K.; Dalgarno, S. J.; Atwood, J. L. *J. Am. Chem. Soc.* **2006**, *128*, 15060.

(5) (a) White, M. A. *NATO ASI Series, Series C: Mathematical and Physical Sciences* **1999**, *539*, 273. (b) White, M. A. In *Properties of Materials*; Oxford University Press: New York, 1999.

(6) (a) Takamizawa, S.; Nakata, E.; Saito, T.; Kojima, K. *CrystEngComm* **2003**, *5*, 411. (b) Takamizawa, S.; Nakaya, E.; Saito, T. *Angew. Chem., Int. Ed.* **2004**, *43*, 1368. (c) Takamizawa, S.; Nakata, E.; Saito, T. *Inorg. Chem. Commun.* **2003**, *6*, 1415. (d) Takamizawa, S.; Nakata, E.; Saito, T. *Chem. Lett.* **2004**, *33*, 538. (e) Takamizawa, S.; Nakata, E.; Saito, T.; Akatsuka, T.; Kojima, K. *CrysEngComm* **2004**, *6*, 197. (f) Takamizawa, S.; Nakata, E. *CrystEngComm* **2005**, *7*, 476. (g) Takamizawa, S.; Nakata, E.; Saito, T.; Akatsuka, T. *Inorg. Chem.* **2005**, *44*, 1421.

(7) Takamizawa, S.; Nakata, E.; Yokoyama, H.; Mochizuki, K.; Mori, W. *Angew. Chem., Int. Ed.* **2003**, *42*, 4331.

(8) (a) Takamizawa, S.; Nakata, E.; Yokoyama, H. *Inorg. Chem. Commun.* **2003**, *6*, 763. (b) Takamizawa, S.; Nakata, E.; Saito, T. *Inorg. Chem. Commun.* **2004**, *7*, 1.

(9) Kottas, G. S.; Clarke, L. I.; Horinek, D.; Michl, J. *Chem. Rev.* **2005**, *105*, 1281, and references therein.

(10) Cotton, F. A.; Walton, R. A. *Multiple Bonds between Metal Atoms*, 2nd ed.; Oxford University Press: New York, 1993.

(11) Takamizawa, S.; Nakata, E.; Akatsuka, T. *Angew. Chem., Int. Ed.* **2006**, *45*, 2216.

Table 1. Crystallographic Data for Single Crystal Host **3** under Various Conditions

complex	**3a**	**3a**	**3a** · 0.49(CO_2)	**3a** · 2(CO_2)	**3b**	**3b**	**3b** · 0.65(CO_2)
pressure	no gas	no gas	CO_2 0.1 MPa	CO_2 1.7 MPa	no gas	no gas	CO_2 0.1 MPa
empirical formula	$C_{34}H_{28}N_2O_8Rh_2$	$C_{34}H_{28}N_2O_8Rh_2$	$C_{34.40}H_{28}N_2O_{8.79}Rh_2$	$C_{36}H_{28}N_2O_{12}Rh_2$	$C_{34}H_{28}Cu_2N_2O_8$	$C_{34}H_{28}Cu_2N_2O_8$	$C_{34.65}H_{28}Cu_2N_2O_{9.29}$
crystal size [mm^3]	0.30 × 0.14 × 0.08	0.30 × 0.14 × 0.08	0.20 × 0.20 × 0.04	0.60 × 0.40 × 0.10	0.30 × 0.08 × 0.04	0.30 × 0.08 × 0.04	0.20 × 0.14 × 0.03
M [g mol^{-1}]	798.40	798.40	815.79	886.42	719.66	719.66	748.05
crystal system	triclinic	triclinic	triclinic	triclinic	triclinic	triclinic	triclinic
space group	$P\bar{1}$	$P\bar{1}$	$P\bar{1}$	$P\bar{1}$	$P\bar{1}$	$P\bar{1}$	$P\bar{1}$
T [K]	298	90	90	90	298	90	90
a [Å]	10.504(3)	10.2633(5)	10.3170(11)	10.453(3)	10.484(3)	10.2611(6)	10.5149(10)
b [Å	10.523(3)	10.4611(5)	10.4309(11)	10.896(4)	10.515(3)	10.4184(6)	10.3425(10)
c [Å]	15.784(5)	15.7171(7)	15.6740(16)	15.659(5)	15.681(5)	15.6335(9)	15.5194(15)
α [deg]	80.233(6)	79.8530(10)	80.248(2)	98.748(7)	81.244(6)	81.1410(10)	82.721(2)
β [deg]	80.818(6)	81.0400(10)	81.189(2)	99.360(7)	82.174(6)	82.3020(10)	82.702(2)
γ [deg]	88.595(7)	87.3630(10)	87.870(2)	90.288(7)	88.840(7)	87.7220(10)	89.957(2)
V [$Å^3$]	1697.3(8)	1640.51(13)	1642.7(3)	1738.4(10)	1692.6(9)	1636.16(16)	1660.4(3)
Z	2	2	2	2	2	2	2
D_{calcd} [g cm^{-3}]	1.562	1.616	1.649	1.693	1.412	1.461	1.496
μ (Mo Kα) [mm^{-1}]	1.024	1.059	1.061	1.017	1.308	1.353	1.339
reflections collected	12569	12203	11960	6305	12023	12143	12301
independent reflections (R_{int})	8266 (0.0172)	8015 (0.0154)	8010 (0.0405)	3616 (0.1195)	8118 (0.0230)	8002 (0.0173)	8135 (0.0410)
goodness of fit	1.076	1.039	1.059	0.952	1.123	1.137	0.986
R1 ($I > 2\sigma$ (all data))	0.0361 (0.0476)	0.0269 (0.0323)	0.0468 (0.0939)	0.1037 (0.1706)	0.0627 (0.0904)	0.0432 (0.0530)	0.0633 (0.1213)
wR2 ($I > 2\sigma$ (all data))	0.0749 (0.0840)	0.0588 (0.0632)	0.0994 (0.1373)	0.2456 (0.2757)	0.1331 (0.1495)	0.0963 (0.1049)	0.1317 (0.1563)
least diff. peak (hole) [e•$Å^{-3}$]	0.767 (−0.550)	0.847 (−0.447)	1.999 (−1.425)	4.755 (−2.672)	0.874 (−0.408)	1.497 (−0.421)	2.000 (−0.683)
void volume per Z [$Å^3$]	70.8	54.0	42.9	133.7	60.4	37.9	70.4
void volume [%]	8.3	6.6	5.2	15.4	7.1	4.6	8.5

For complexes **1**−**2**, see Supporting Information.

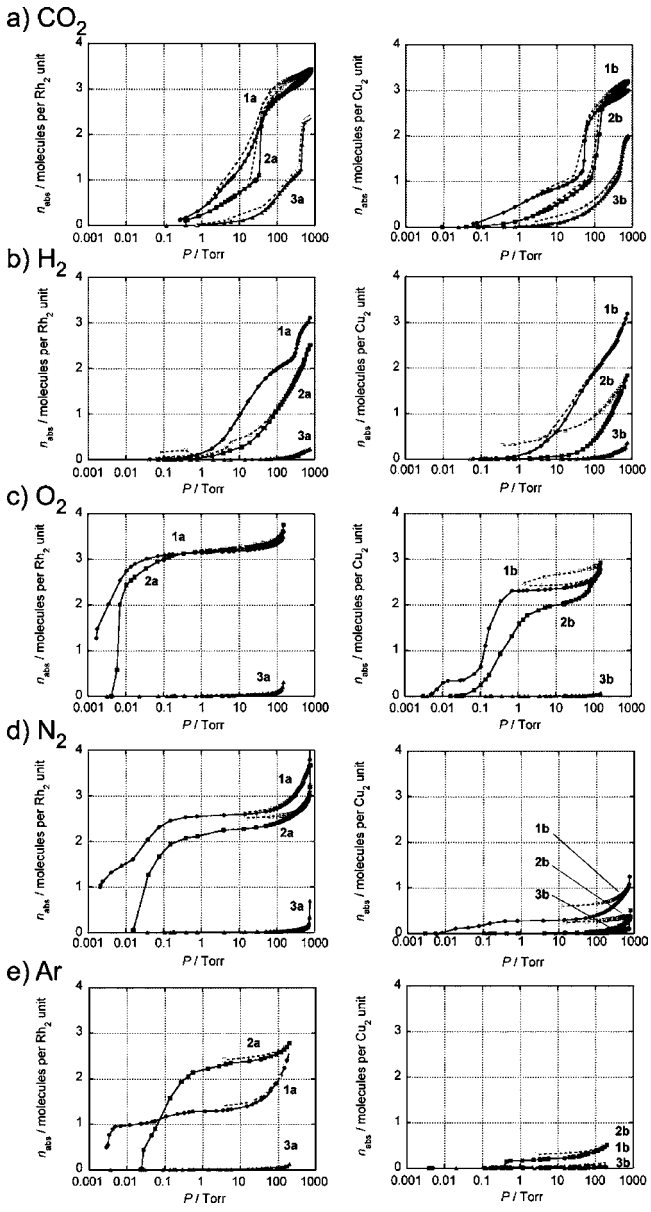

Figure 1. Adsorption isotherms of CO_2 (a) at 195 K and H_2 (b), O_2 (c), N_2 (d), and Ar (e) at 77 K for **1a**-**3a** (left column) and **1b**-**3b** (right column).

Gas Adsorption Properties. The gas adsorption capacities of all adsorbents **1**-**3** were characterized for CO_2, H_2, N_2, O_2, and Ar at 195 K for CO_2 and at 77 K for all the others (Figure 1).[12] In spite of the addition of the methyl group in the void space, all crystal hosts adsorbed CO_2 gases with a similar saturated amount (3 molecules per M_2 unit for **1a**,[7] **1b**,[8] **2a**,[11] **2b** and 2 molecules per M_2 unit for **3a** and **3b**). The abrupt increase of the isotherm curves were clearly observed at the same adsorption amount (1 CO_2/M_2 unit) but at different CO_2 pressures (10 Torr for **1a**, 54 Torr for **1b**, 36 Torr for **2a**, 120 Torr for **2b**, 465 Torr for **3a**, and 520 Torr for **3b**) as was also observed for isobar curves (Figure S15, Supporting Information). In the case of H_2[13] and O_2 gases, **1a**, **1b**,[6e] **2a**, and **2b** adsorbed the gases at almost the same, relatively low pressure and showed smooth and reversible adsorption properties. In contrast, in the case of N_2 and Ar gases, the Rh complexes (**1a**,[14,15] **2a**) showed smooth adsorption and reached an saturated amount (3 molecules per Rh_2 unit) while the Cu complexes (**1b**, **2b**) did not adsorb N_2 and Ar gases.[16] This fact suggests that gas selectivity can depend on the type of metal center.

Solid-state NMR Study of Molecular Motion. The host series in this study adsorbed gases through narrow channels. The initial pressure to make the gas molecules enter the channels depended on the substitution number of the methyl group. To reveal this adsorption characteristic, temperature variations of the solid-state ^{1}H NMR spectra of $[Rh_2(O_2C-C_6H_5)_4(pyz)]_n$ (**1a**) and its partially deuterated analogue $[Rh_2(O_2C-C_6D_5)_4(pyz)]_n$ (**1a′**) under N_2 gas flow were first measured (Figure S14). A motional narrowing of the spectral width of ^{1}H NMR was observed between 125 and 300 K for **1a** whereas almost no narrowing was detected for **1a′**, indicating that the motion of the phenyl group of the benzoate ligand is thermally activated in this temperature region (also see Figure S15, Supporting Information). The 180°-flip motions of the phenyl group around the C−C bond were confirmed by the ^{2}H NMR spectrum of **1a′** (left column of Figure 2a). A typical Pake doublet pattern was observed at 200 K for a deuterium atom of a phenyl group without motion.[17] The line shape changed with increasing temperature to show a 180°-flip motion of the phenyl group, which was rapid enough at 295 K. The spectral line shape was simulated to determine the rate of the motion at each temperature (right column of Figure 2a). An Arrhenius plot of the rate constant gave an activation energy of 38 ± 4 kJ mol^{-1} for the 180°-flip motion of the phenyl group. Although the rotational motion of the pyrazine ring around the N−N axis shows almost no fluctuation of intramolecular dipole interactions between adjacent protons and the ^{1}H NMR spectrum is almost independent of the rotational motion around the N−N axis, the ^{2}H NMR spectrum of the pyrazine-deuterated analogue $[Rh_2(O_2C-C_6H_5)_4(pyz\text{-}d_4)]_n$ (**1a″**) clearly revealed the 180°-flip motion of the pyrazine ring around the N−N axis (Figure 2b). The activation energy of this motion (49 ± 4 kJ mol^{-1}) was greater than the activation energy of the 180°-flip motion of the phenyl group (Figure S16, Supporting Information).

The rapid 180°-flip motion of the phenyl ring at room temperature, which is similar to the motion of a "rotating door," seems to play an important role for gas inclusion into the crystalline lattice of **1a** (**1a′**), particularly near the initiation of gas adsorption. To clarify this point, solid-state NMR of the host under 0.1 MPa of CO_2 pressure was also measured for **1a′**. The ^{2}H NMR spectrum shows that the rate of the 180°-flip motion of the phenyl ring under 0.1 MPa of CO_2 pressure is smaller than that of the crystals before adsorption[18] (Figure 3; also see Figure S17, Supporting Information). The crystal of **1a** before adsorption is in the monoclinic phase (α phase), which

(12) Only slight amount of gases (CO_2, H_2, O_2, N_2, and Ar) was adsorbed in these adsorbents around room temperature at 0.1 MPa. For the detail of adsorption behavior of **1b** for CO_2 gas under high pressure conditions, see: Takamizawa, S.; Takasaki, Y.; Miyake, R. *Chem. Commun.* **2009**, 6625.

(13) The number of included H_2 gases was not saturated at the measured condition (77 K, 0.1 MPa).

(14) Kachi-Terajiama, C.; Akatsuka, T.; Kohbara, M.; Takamizawa, S. *Chem. Asia. J.* **2007**, *2*, 40.

(15) Ar gas-adsorbing behavior under high-pressure conditions was reported for **1a** and **1b**:Ueda, T.; Kurokawa, K.; Eguchi, T.; Kachi-Terajima, C.; Takamizawa, S. *J. Phys. Chem. C* **2007**, *111*, 1524.

(16) **1b** adsorbed N_2 or Ar gas at more high temperature under high pressure.

(17) *Nuclear Magnetic Resonance Probes of Molecular Dynamics*; Tycko, R., Ed.; Kluwer Academic Publishers: The Netherlands, 1994.

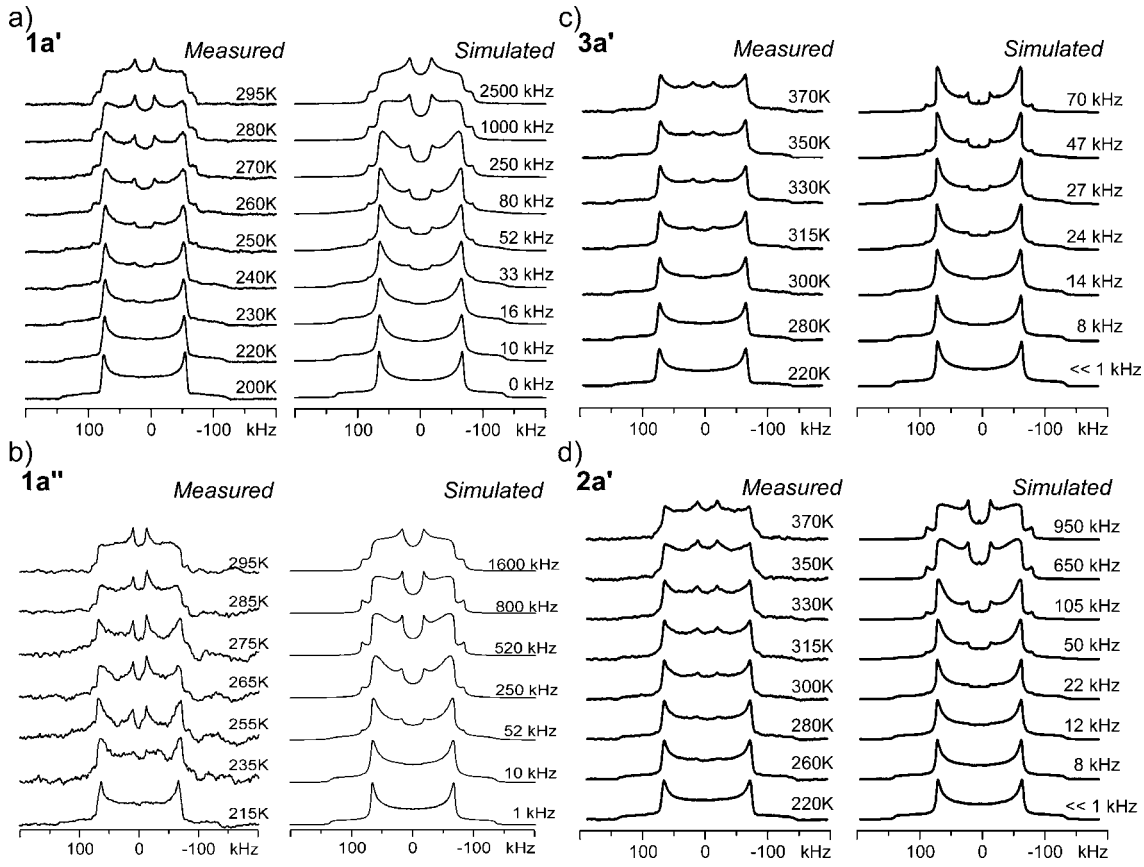

Figure 2. Temperature variation of ^{2}H NMR spectrum (left) with simulated spectrum (right): (a) spectrum of phenyl-deuterated sample $[Rh_2(O_2C-C_6D_5)_4(pyz)]_n$ (**1a′**), (b) spectrum of pyrazine-deuterated sample $[Rh_2(O_2C-C_6H_5)_4(pyz\text{-}d_4)]_n$ (**1a″**), and (c, d) spectra of phenyl-deuterated samples $[Rh_2(O_2C-C_6D_5)_4(2,3\text{-mpyz})]_n$ (**3a′**) (c) and $[Rh_2(O_2C-C_6D_5)_4(2\text{-mpyz})]_n$ (**2a′**) (d) under N_2 gas flow. Indications of the simulated spectrum in which rates of the 180°-flip motion of the phenyl group around the C−C bond (a, c, d) and 180°-flip motion of the pyrazine ring around the N−N axis (b).

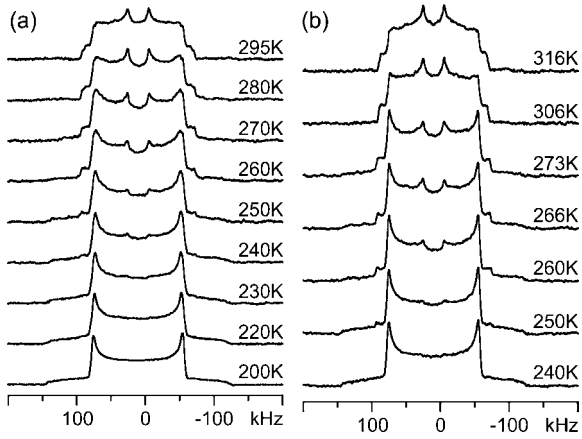

Figure 3. Comparison of ^{2}H NMR spectrum of $[Rh_2(O_2C-C_6D_5)_4(pyz)]_n$ (**1a′**) between different conditions under N_2 gas (a) and under 0.1 MPa of CO_2 gas (b).

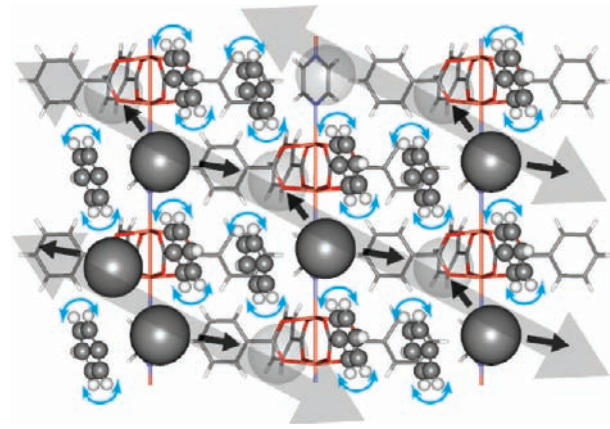

Figure 4. Schematic diagram of the "rotating door" motion of the flipping benzene rings of the host skeleton consisting of inner channel walls.

has small spaces to contain the CO_2 molecules. Once the CO_2 molecules enter the lattice, the phenyl rings interact with the CO_2 molecules to stabilize the channel structure by expanding the lattice after which the crystal transforms into the triclinic phase (β phase). As reported previously[7] (also see Crystal structure section), phenyl rings closely interact with included CO_2 molecules. These facts suggest that the rotational motion would be affected by the absorbed CO_2 molecules (Figure 4).

Since the crystals of **3a** adsorbed a much smaller amount of gas molecules at 0.1 MPa as compared with those of **1a**, the dynamic properties of the phenyl rings and the dimethylpyrazine moieties are of interest. We also measured the solid-state ^{1}H and ^{2}H NMR spectra of phenyl-deuterated **3a** (**3a′**) to clarify the motional property of these groups individually. Figure 2c shows the temperature dependence of the observed ^{2}H NMR spectrum of **3a′** and the simulation. 180°-flip motion of the phenyl group is slower than 100 kHz even at an elevated temperature of 370 K and only 14 kHz at 300 K. The rate of the 180°-flip motion of the phenyl group of phenyl-deuterated **2a** (**2a′**) was between **1a′** and **3a′**, but closer to **3a′** (Figure 2d). Solid-state ^{1}H NMR spectra of **2a′** and **3a′** were almost

independent of temperature between 120 and 370 K (Figure S18, Supporting Information). Each spectrum consisted of a typical spectral component line shape of a rapidly rotating methyl group, of which the three protons have a total nuclear spin of 3/2 and exhibit a characteristic dipolar line shape,[19] and a spectrum of ring protons. These different types of protons show slightly different shifts, probably due to the magnetism of the Rh ions. This result suggests that, unlike the case of **1a′**, 2-methylpyrazine of **2a′** and 2,3-dimethylpyrazine of **3a′** do not undergo 180°-flip motion around the axis of Rh−N—N−Rh. Thus, the near immobility in the flip motions of the phenyl ring and pyrazine moiety seems to correspond to the increase of the initial pressure and critical pressure of gas adsorption with the increase of substitution in the host series (**1a**−**3a**).

Crystal Structures of CO_2 Inclusions of 1a and 1b. To clarify the relationship between host structures, including structural transformation and adsorption ability, the crystal structures of CO_2-included complexes (denoted as CO_2-included crystal) were studied because CO_2 gas was well adsorbed by all of the complexes under moderate conditions.

The structures of saturated inclusion crystals **1a**·3(CO_2) and **1b**·3(CO_2) were determined at 90 K under a CO_2 atmosphere (Table S1, Supporting Information). The CO_2-included crystals of **1a** and **1b** are isostructural. The structural transformation from monoclinic (*C*2/*c* (∼<200 K for **1a**), *C*2/m (∼>200 K for **1a**)) to triclinic ($P\bar{1}$) is induced by the CO_2 adsorption and, as was described in previous papers,[7,8] this transformation is accompanied by the expansion of 1-D channels through (1) a slide in the opposite direction of the neighboring chains; (2) a tilt of the $\pi-\pi$ stacked phenyl rings; and (3) an extension of the interchain distances, as depicted in Figure 5b. The 1-D channels in the transited structure are formed along the *b*-axis of the crystal while the 1-D chain of the metal complex is formed along the *a*-axis of the crystal. After the transformation, the ratio of the void volume[20] in the crystal at 90 K increased (**1a**: from 16.2% to 20.2%, **1b**: from 14.3% to 20.2%). The straight 1-D skeletons of the **1a** and **1b** crystals before adsorption (denoted as nonincluded crystal) were maintained after the transformation. A large structural change was found in the π-stacked phenyl rings where the torsion angle between (M−M axis)·(phenyl plane of $\pi-\pi$ stacked benzoate) changed by 11.1° and 24.9° from the nonincluded crystals of **1a** and **1b** at 298 K (from those at 90 K, 24.9º for **1a** and 26.0º for **1b**, please refer to Tables S3,4), respectively. As shown in Figure 5c, adsorbed CO_2 molecules in **1a** are arranged along the 1-D channel. The arrangements of the CO_2 molecules in **1b** were almost the same as those in **1a**. A repeating [A−A−B] arrangement of CO_2 molecules was formed with the two different molecular axes (A (O1S−C1S−O2S) and B (O3S−C2−O3S$^{\#}$) (symmetry operation $^{\#} = -x, 2 - y, 2 - z$)) that are almost parallel and perpendicular to the channel direction, respectively. Considering the electric quadrupole moment of the CO_2 molecules, the most stable arrangement of 2 CO_2 molecules is in a parallel orientation (denoted as parallel array A-A) and the second most stable arrangement is in a perpendicular orientation (denoted as perpendicular array A−B).[21] The CO_2 molecules were densely included in the channel with a combination of the above two array styles. In the CO_2 arrangement, close contacts between host and guest and between guests are found and are almost the same for both complexes **1a** and **1b**, as shown in Figures S7−8, Supporting Information.

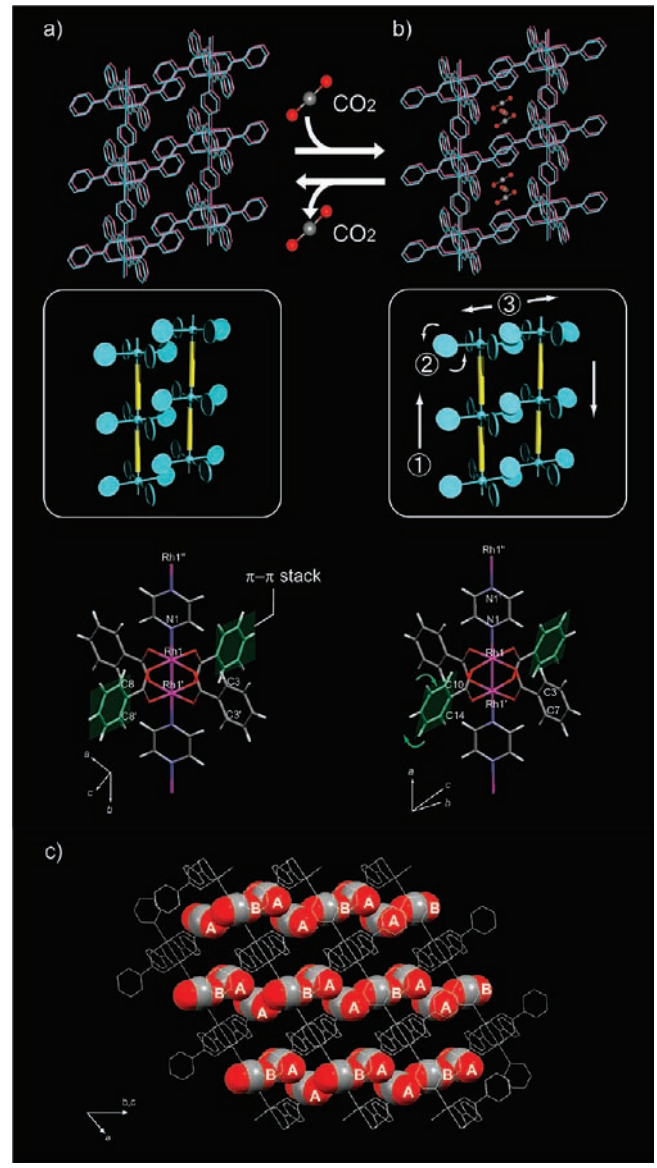

Figure 5. Schematic diagrams of channel transformation by CO_2 adsorption. Nonincluded (a) and inclusion (b) crystals of **1a**: crystal packing structures (upper step), conceptual diagrams showing structural changes of the 1-D chain (middle step), and capped stick models of the 1-D chain (bottom step). (c) CO_2 array in crystal structure along the channel axis.

Crystal Structures of CO_2 Inclusions of 2a and 2b. Although the void volume of the **2a** and **2b** crystals was partially occupied by the additional methyl group on the pyrazine ring, a saturation state of 3 CO_2 molecules per M_2 unit was achieved at 90 K under a CO_2 atmosphere (Table S2, Supporting Information). Compounds **2a** and **2b** are isostructural and belong to the triclinic $P\bar{1}$ space group before and after CO_2 adsorption although the zigzag chain of the host structures was dramatically changed to a straight chain after CO_2 adsorption (see Tables

(18) It is noted that a simulation of the ^{2}H NMR spectrum by assuming a uniform rate constant of motion failed to fit the experimental results in the intermediate temperature region near 300 K. This result suggests a distribution of the rate of motion because of nonstoichiometric inclusion of CO_2 molecules at the temperature region under 0.1 MPa of CO_2.

(19) Takeda, S.; Chihara, H. *J. Magn. Reson.* **1984**, *56*, 448.

(20) The void volume (or void space) for CO_2-included crystals was estimated from the host structure after excluding included CO_2 gases.

(21) Kihara, T.; Koide, A. *Adv. Chem. Phys.* **1975**, *33*, 51.

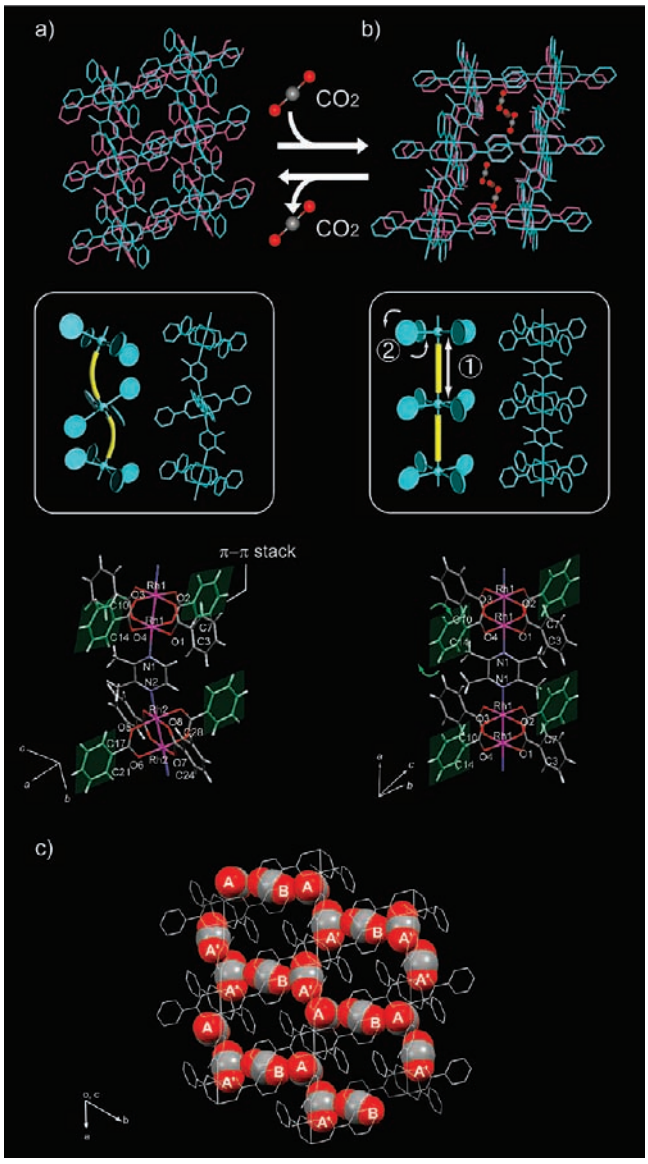

Figure 6. Schematic diagrams of channel transformation by CO_2 adsorption. Nonincluded (a) and inclusion (b) crystals of **2a**: crystal packing structures (upper step), conceptual diagrams showing structural changes of the 1-D chain (middle step), and capped stick models of the 1-D chain (bottom step). (c) CO_2 array in crystal structure along the channel axis.

S3−S4, Supporting Information and Figure 6a, b). At 90 K, the bend angles of the zigzag chain were 169.74° for **2a** and 169.88° for **2b** before CO_2 adsorption and were both changed to 180° after CO_2 adsorption.[22] As the zigzag chain was stretched, the tilt angles of the π-stacked phenyl rings from the M−M axis changed by 2.4° and 7.3° for **2a** and 1.3° and 5.3° for **2b**. Thus, in **2a** and **2b**, the transformation of the host structures should be induced by the stretch of the 1-D chain and the tilt of the $\pi-\pi$ stacked phenyl rings, as was observed in the 2-ethylpyrazine derivative.[23] Consequently, the quadruple $\pi-\pi$ stacking of the phenyl rings found in the nonincluded crystals was separated into two double-stacking ones to create additional space for CO_2 adsorption. Thus, elongation of the distance between the phenyl rings by the adsorbed CO_2 molecules should be one of the important factors affecting the transformation of the crystal structure (Figure S6, Supporting Information). By structural transformation, **2a** and **2b** efficiently increase the space for adsorption compared with the increase of crystal cell volume and achieved 3 CO_2 inclusion, which is the same amount as with **1a** and **1b**.

The CO_2 molecules are densely arranged along the 1-D channel, which is similar to the complexes of **1a** and **1b**. However, adsorbed CO_2 molecules (A′) were disordered depending on the disordered positions of the methyl group (Figure 6c and Figures S9−10, Supporting Information), which decrease the parallel array of CO_2.[24]

Crystal Structures of CO_2 Inclusions of 3a and 3b. By introducing 2,3-dimethylpyrazine instead of 2-methylpyrazine of **2a** and **2b**, the number of CO_2 molecules included in **3a** and **3b** was decreased: **3a**·0.49(CO_2), **3b**·0.65(CO_2) under 0.1 MPa of CO_2 and **3a**·2(CO_2) under 1.7 MPa of CO_2 gas, which were determined by single-crystal X-ray diffraction experiments at 90 K (Table 1). Under pressurized CO_2 gas (1.7 MPa at 298 K), the composition of **3a**·2(CO_2) is in good agreement with those determined by gas adsorption isotherm measurements.[25]

In contrast to **2a** and **2b**, the bend of the zigzag chain remained after inclusion in **3a** and **3b**. Two methyl substituents in the ortho positions on the pyrazine moiety for **3** clearly showed inhibition of structural change in the host skeleton, keeping the zigzag chain and the quadruple $\pi-\pi$ stacking of phenyl rings during the gas adsorption process. For **3a**·2(CO_2), the void volume[20] was increased by 8.8% (79.7 Å^3 per M_2 unit) from that of the nonincluded crystal of **3a**, which is smaller than are those in **1** and **2**. However, the crystal volume showed a smaller change (6.0% (48.9 Å^3 per M_2 unit) increase) than the increase in void volume, indicating that the tilt and slip of the stacked phenyl rings effectively generate void space to adjust to the included guest molecules to suppress the large change of crystal volume (Figure 7b).

A small quantity of CO_2 molecules was incorporated under atmospheric conditions in **3a** and **3b**, which corresponds to a limited space in a channel compared with other host crystals. In the crystal filled with CO_2 under 1.7 MPa, additional CO_2 molecules were inserted between the first accommodated guest molecules under 0.1 MPa. In this crystal, the CO_2 molecular axes (molecules A (O1S−C1S−O2S) and B (O2S−C3S−O4S)) are in two different directions and are almost perpendicular to one another (Figure 7c and Figure S11b, Supporting Information). This arrangement was completely different from those of **1** and **2**, suggesting that the CO_2 arrangement can be tuned by modification inside the channel. In the CO_2 arrangement, the shortest interguest distance (C···O) between the A and B molecules is 3.02(4) Å, which forms a tetramer of CO_2 molecules within an isolated cavity. (Figures S6, S11 for **3a**, Figure S12 for **3b**, and Table S5 for **3a**, **b**, Supporting Information).

Thermal Study of Structural Transformation. Crystal structural analysis revealed that the addition of methyl groups on

(22) In this straight chain, disordered methyl groups were found on both sides of the pyrazine backbone while they were located on only one side before the transition (the bottom step of Figure 6a, b).
(23) Takamizawa, S.; Kojima, K.; Akatsuka, T. *Inorg. Chem.* **2006**, *45*, 4580.
(24) The two different molecular axes of the CO_2 molecules are, however, observed at sites of A (A: (O1A−C1A−O2A) and A′ (O1B−C1B−O2B)), which are the disordered molecules with site occupancies of 50% in the same location as a cavity. (Refer to Figure S9.)
(25) The number of absorbed CO_2 molecules observed in the X-ray structural analysis at 90 K was considerably low as compared with the 2 molecules found in the adsorption measurement at 195 K under 0.1 MPa (see Figure 1a) due to a decrease of the inner pressure of the sealed glass capillary for the X-ray experiment caused by cooling the sample from 298 to 90 K.

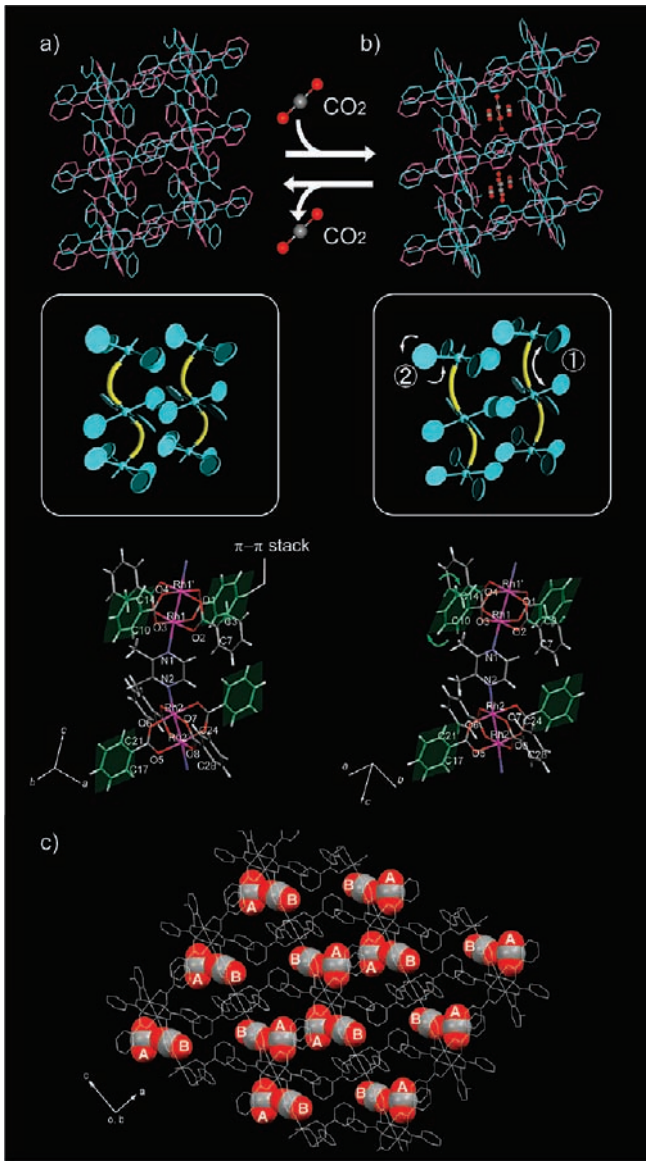

Figure 7. Schematic diagrams of channel transformation by CO_2 adsorption. Nonincluded (a) and inclusion (b) crystals of **3a**: crystal packing structures (upper step), conceptual diagrams showing structural changes of the 1-D chain (middle step), and capped stick models of the 1-D chain (bottom step). (c) CO_2 array in crystal structure along the channel axis.

the pyrazine ring induced a characteristic change of the host structural transformation during CO_2 adsorption. To clarify the relationship between the bulk transition and characteristic adsorption of CO_2 molecules, differential scanning calorimetry (DSC) measurements were performed under various mixtures of CO_2/N_2 atmospheres. The temperature of the measurements ranged from 50 to −40 °C for **1a**,[7] −30 to −90 °C for **1b**,[8a] −20 to −90 °C for **2a**, −30 to −90 °C for **2b**, −20 to −100 °C for **3a**, and −40 to −100 °C for **3b** (Figure 8). We found that the temperature of the heat anomaly in the DSC curve depended on the partial pressure of CO_2 and agreed with the temperature of the abrupt change of the amount of CO_2 adsorption that appeared in the isobar measurements under 0.1 MPa of a pure CO_2 atmosphere (Figure S13, Supporting Information). This result indicates that the bulk transition of the crystal is accompanied by the rapid increase in CO_2 adsorption.[7,8a]

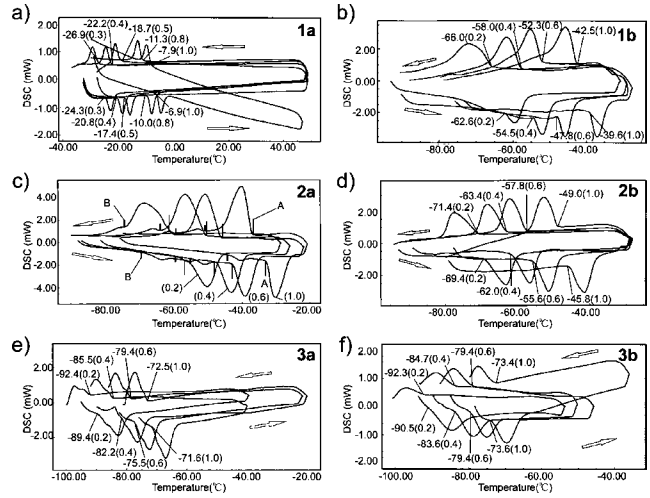

Figure 8. DSC cyclic patterns of crystals **1**−**3** under ambient pressure with different CO_2/N_2 mixtures at a scanning rate of 5 °C min^{-1} for Rh complexes **1a** (a), **2a** (c), and **3a** (e), and for Cu complexes **1b** (b), **2b** (d), and **3b** (f).

The enthalpy of the bulk transition, which was determined from the integrated DSC peak (total enthalpy: ΔH_{trans}), consists of the adsorption enthalpy of the additional CO_2, the enthalpy of the rearrangement of previously included CO_2, and the structural change of the host lattice. The total enthalpy ΔH_{trans} obtained from the heating processes of DSC measurements is listed in Table 2 for all compounds.[26] Compound **1a** showed considerably small transition enthalpy (ΔH_{trans}: ∼5 kJ mol^{-1}) compared with that of the other complexes (ΔH_{trans}: 13−41 kJ mol^{-1}). Since the structural difference of the CO_2 arrangements between the Rh complexes and the Cu complexes was small, as described in the Crystal structure section, this difference would correlate with the relatively small change (from *C*2/*m* to $P\bar{1}$, also refer to Tables S3−S4, Supporting Information) of the crystal structure of **1a** through CO_2 adsorption.[27] The large values of ΔH_{trans} (23−41 kJ mol^{-1}) observed for **2a** and **2b** are probably related to the large structural changes of the stretching of the zigzag chains. For **3a** and **3b**, the small structural changes of the zigzag chain show the smaller values of ΔH_{trans} (13−22 kJ mol^{-1}) than those for **2a** and **2b**.

Since the observed transition temperature varied systematically with the partial CO_2 pressure for all samples, we tried to determine what kind of relationship exists between the transition temperature and the partial pressure of CO_2 gas for each sample. A plot of the logarithms of the partial pressure of CO_2 gas as a function of the reciprocal of absolute transition temperature gave a linear relationship (Figure 9). This result is very similar to the behavior of the solid−gas (or liquid−gas) phase boundary of single-component materials and can be explained by the Clausius−Clapeyron equation. The relationship strongly suggests that the observed transition can be regarded as a pseudo phase transition from the CO_2 aggregate included within the host lattice to the gas state (quasi-solid−gas phase transition) of the aggregated CO_2 cluster. Interestingly, the values of

(26) Evaluation of ΔH_{trans} for the cooling process was difficult because of supercooling of the transition and limited temperature region of the measurements, i.e., $T > -95$°C.

(27) Although **1a** transits its crystal phase from *C*2/*m* to *C*2/*c* by a cooling process (around−80°C), the DSC peak was assigned as crystal transformation from *C*2/*m* to $P\bar{1}$ accompanying CO_2 adsorption because the observed temperature (−7 to ∼−29°C) was higher than the transition temperature.

Table 2. Calorimetric Data and Estimated Thermal Parameters for **1a**−**3b** from DSC Measurements

1a[7]	P_{CO2}	T/°C (heating)	ΔH_{trans}[a] (kJ mol^{-1}) (heating)	ΔH_{iso}[b] (kJ mol^{-1}) (heating)
	1.0	−6.9	5.4	43.4
	0.8	−10.0	5.1	
	0.7	−11.9	5.0	
	0.6	−14.7	4.8	
	0.5	−17.4	5.4	
	0.4	−20.8	4.9	
	0.3	−22.9	5.0	
	0.2	−28.8	4.7	
2a	P_{CO2}	T/°C (heating)	ΔH_{trans} (kJ mol^{-1}) (heating)	ΔH_{iso} (kJ mol^{-1}) (heating)
A	1.0	−33.2	23.2	36.6
	0.6	−43.0	23.6	
	0.4	−47.3	24.1	
	0.2	−56.1	23.8	
B	1.0	−51.5	1.6	30.5
	0.6	−60.2	2.0	
	0.4	−64.4	1.9	
	0.2	−73.7	2.1	
3a	P_{CO2}	T/°C (heating)	ΔH_{trans} (kJ mol^{-1}) (heating)	ΔH_{iso} (kJ mol^{-1}) (heating)
	1.0	−71.6	21.8	32.3
	0.6	−75.5	20.6	
	0.4	−82.2	17.9	
	0.2	−89.4	19.5	
1b[8a]	P_{CO2}	T/°C (heating)	ΔH_{trans} (kJ mol^{-1}) (heating)	ΔH_{iso} (kJ mol^{-1}) (heating)
	1.0	−39.6	15.8	33.7
	0.6	−47.8	23.4	
	0.4	−54.5	30.5	
	0.2	−62.6	24.0	
2b	P_{CO2}	T/°C (heating)	ΔH_{trans} (kJ mol^{-1}) (heating)	ΔH_{iso} (kJ mol^{-1}) (heating)
	1.0	−45.8	38.6	31.1
	0.6	−55.6	39.3	
	0.4	−62.0	39.5	
	0.2	−69.4	41.4	
3b	P_{CO2}	T/°C (heating)	ΔH_{trans} (kJ mol^{-1}) (heating)	ΔH_{iso} (kJ mol^{-1}) (heating)
	1.0	−73.6	14.0	35.3
	0.6	−79.4	12.9	
	0.4	−83.6	12.9	
	0.2	−90.5	12.6	

[a] Estimated value from area of the DSC peak. [b] The isosteric enthalpy of adsorption of CO_2 gas (ΔH_{iso}) was calculated from the slope of the linear Clausius−Clapeyron correlation ($d(\ln P)/d(1/T) = \Delta H_{iso}/R$ for the adsorption process, where R denotes the gas constant).

enthalpy (ΔH_{iso}) estimated from the Clausius−Clapeyron equation are almost constant (31−41 kJ mol^{-1}) irrespective of different complexes (Table 2, also see Table S6, Supporting Information) in contrast to the considerably different values of ΔH_{trans} determined from DSC measurements. This enthalpy ΔH_{iso} dominantly consists of guest−guest and local host−guest interactions in a cavity of each host lattice in the first approximation and does not directly include the enthalpy of the long-range structural change of the host lattice, which is largely different among the host complexes. The enthalpy ΔH_{iso} is larger than the sublimation enthalpy of solid CO_2 (25 kJ/mol),

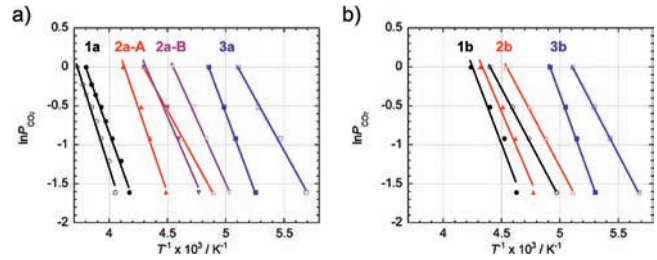

Figure 9. CO_2 partial pressure (ln P_{CO2}) vs transition temperature (T^{-1}) plotted for Rh complexes (a) and for Cu complexes (b): (open symbol: heating step, filled symbol: cooling step).

indicating strong interaction between CO_2 molecules and the local host lattice. The enthalpy ΔH_{trans} of the bulk structural transition induced by additional adsorption of CO_2 is almost independent of the partial pressure of CO_2 for each complex (Table 2). This result indicates that the same structural transition occurs at different temperatures depending on the different critical pressure of CO_2 in the same flexible host. The difference between ΔH_{trans} and ΔH_{iso} mostly corresponds to the enthalpy of the long-range structural change of the host lattice. The negative values in **1** and **2** indicate that the host lattice itself becomes unstable by adsorbing CO_2 molecules (Table S6, Supporting Information).

Structural transformation occurred at the adsorption amount of 1 CO_2 molecule per M_2 unit regarded as a critical adsorption amount, while the corresponding critical pressure varies as described in the section of Gas adsorption properties. Consequently, we propose that this phenomenon could be called "mass (amount of adsorbed guest) induced phase transition",[6g] which is distinguished from the well-known temperature- or pressure-induced transition because the transformation is triggered by the level of gas adsorption. Thus, there is a possibility of controlling adsorption property by means of structural transformation in a flexible host system that has great capability of being chemically modified.

Conclusion

We have succeeded in the synthesis of single-crystal adsorbents **1**−**3** with different metals (Rh (**a**) and Cu (**b**)) and/or substituents (-H, -Me, and -2Me) on the pyrazine ring and determining the absorbency of various gases (CO_2, H_2, O_2, N_2, and Ar). The difference in metal replacement on adsorbency was clearly observed for N_2 and Ar gases. Solid-state NMR measurement indicated the existence of local motion, which promotes gas diffusion through narrow channels by 180°-flip motions of the aromatic rings of the host skeleton. The silence of these motions in **2a** and **3a** suggests the importance of the rotational motion of the phenyl ring for smooth adsorption at a relatively low-pressure region. By introducing the substituent into host skeletons, steric hindrance in the host skeletons reduced the void space, but the adsorption amount kept similar values by changing the manner of the transformation of the host structure. These results revealed a strong correlation between the manner of host structural transformation and gas adsorption behavior. The structural transformation by CO_2 gas adsorption is confirmed by a transition from single-crystal to single-crystal states accompanying adsorption leaps. Since the structural transformations occurred when the adsorption amount reached approximately 1 molecule per M_2 unit, the adsorption amount should be important triggers for dynamic adsorption behaviors. Thus, control of host transformability enables tuning of the

dynamic adsorption properties and guest arrays. Such adsorption properties of the host, which are induced by correlation between structural transformation and gas adsorption, will be expected to provide the sort of novel diffusivity and dynamic selectivity that will contribute to new strategies in gas storage/release and separation. In addition, this study would help in understanding the principle of the dynamic adsorption mechanism generally applicable for other flexible porous materials, which has recently been the subject of considerable attention.[2–4]

Experimental Section

Preparation of Rhodium(II) Complexes (1a−3a). An acetonitrile solution (20 cm^3) of rhodium(II) benzoate [$Rh(II)_2(O_2CPh)_4$] (20.0 mg, 29.0 μmol) was allowed to stand at room temperature with a linking ligand vapor (pyrazine, 2-methylpyrazine, 2,3-dimethylpyrazine). After one month, polymerized complexes **1a**−**3a** had crystallized in the form of reddish-orange plates in high yields. The crystals were collected by filtration, washed with methanol, and air-dried. For $[Rh_2(O_2CPh)_4(pyz)]$ (**1a**[28]) (67% (15.0 mg) isolated yield): Anal. Calcd for $C_{32}H_{24}N_2O_8Rh_2$: C 49.89; H 3.14; N 3.64%. Found: C 49.53; H 3.18; N 3.72%. For $[Rh_2(O_2CPh)_4(2\text{-mpyz})]$ (**2a**[11]) (61% (13.8 mg)): Anal. Calcd for $C_{33}H_{26}N_2O_8Rh_2$: C 50.35; H 3.34; N 3.57%. Found: C 49.99; H 3.31; N 3.62%. For $[Rh_2(O_2CPh)_4(2,3\text{-dmpyz})]$ (**3a**) (82% (18.9 mg)): Anal. Calcd for $C_{34}H_{28}N_2O_8Rh_2$: C 51.15; H 3.54; N 3.51%. Found: C 50.23; H 3.55; N 3.40%.

Preparation of Copper(II) Complexes (1b−3b). A methanol solution (80 cm^3) of copper(II) acetate monohydrate (80 mg, 0.40 mmol) and benzoic acid (117.2 mg, 0.96 mmol) was allowed to stand for several days with the slow diffusion of pyrazine (pyz, 2-mpyz, 2,3-dmpyz) vapor. Polymerized complexes of **1b**−**3b** crystallized in the form of blue plates in high yields. The crystals were washed with a slight amount of methanol and air-dried. For $[Cu_2(O_2CPh)_4(pyz)]$(**1b**[8a]) (59%, (12.2 mg)): Anal. Calcd for $C_{32}H_{24}N_2O_8Cu_2$: C 55.57; H 3.50; N 4.05%. Found: C 54.43; H 3.44; N 4.17%. For $[Cu_2(O_2CPh)_4(2\text{-mpyz})]$(**2b**) (57%, (11.7 mg)): Anal. Calcd for $C_{33}H_{26}N_2O_8Cu_2$: C 56.17; H 3.71; N 3.97%. Found: C 55.58; H 3.61; N 4.00%. For $[Cu_2(O_2CPh)_4(2,3\text{-dmpyz})]$(**3b**) (74%, (16.0 mg)): Anal. Calcd for $C_{34}H_{28}N_2O_8Cu_2$: C 56.74; H 3.92; N 3.89%. Found: C 55.70; H 3.86; N 4.01%.

Preparation of Deuterized 1a−3a Complexes (1a′, 1a″, 2a′, 3a′). Deuterized benzoate complexes $[Rh_2(O_2C-C_6D_5)_4(R\text{-pyz})]_n$ (R = H (**1a′**), 2-mpyz (**2a′**), 2,3-dmpyz (**3a′**)) and deuterized pyrazine complex $[Rh_2(O_2C-C_6H_5)_4(pyz\text{-}d_4)]_n$ (**1a″**) were synthesized by the same method using corresponding deuterized ligands.

Single-Crystal X-ray Diffraction Experiment. All single-crystal X-ray analyses were performed on a Bruker SMART APEX CCD area detector using graphite-monochromated Mo−Kα radiation (λ = 0.71073 Å) with a nitrogen flow temperature controller. (Although the crystal structures for **1a** and **1b** were described in our previous studies (listed in references[7] and[8]), listed data were unified by reinvestigation using the same diffractometer.) Data for nonincluded crystals were collected at 298 and 90 K under atmospheric conditions without a guest gas. The CO_2-inclusion structures were determined under CO_2 atmospheric conditions for **2a**, **2b**, **3a**, and **3b** and under forcible CO_2 conditions for **3a**. All single crystals except **3a** were sealed in a glass capillary with an ambient pressure of CO_2 gas at room temperature. A single crystal of **3a** was sealed in a glass capillary with solid CO_2 using a liquid nitrogen bath. The inner pressure at room temperature was estimated to be ~1.7 MPa by the ratio of the volume of the solid CO_2 and the inner space; the data was measured at 90 K. Although a small amount of solid CO_2 sometimes emerged in the capillary during the cooling step, its reflection spots were weak and did not spatially interfere with the reflection peaks from the crystal. Face-indexed absorption corrections were made using the Bruker XPREP program. Empirical absorption corrections were applied using the SADABS program. The structures were solved by direct methods (SHELXS-97) and refined by full-matrix least-squares calculations on F^2 (SHELXL-97) using the SHELX-TL software package. Non-hydrogen atoms were refined anisotropically; hydrogen atoms were fixed at calculated positions and refined using a riding model. The crystallographic data of the structure determinations for nonincluded and CO_2-inclusion crystals collected under different conditions are summarized in Tables 1 and S1−S2, Supporting Information. CCDC-758535-758551 contains the supplementary crystallographic data for this paper. (The reinvestigated crystal structural data of **1b** without CO_2 gas was already reported in reference.[29])

Physical Measurements. The gases used during the physical measurements were CO_2 (99.995% purity), H_2 (99.99% purity), N_2 (99.999% purity), O_2 (99.99% purity), and Ar (99.9995% purity). Gas adsorption isotherm measurements for CO_2, H_2, N_2, O_2, and Ar were performed on a Quantachrome Autosorb-1 MP by volumetric method at 195 K for CO_2 and 77 K for H_2, N_2, O_2, and Ar. The measured pressure ranges were from 0.002 to 154 Torr (O_2), 0.002 to 798 Torr (N_2), 0.002 to 201 Torr (Ar), 0.044 to 760 Torr (H_2), and 0.001 to 809 Torr (CO_2). Differential scanning calorimetry (DSC) measurements were recorded on a Shimadzu DSC-60 under ambient pressure with different CO_2/N_2 mixtures at a scanning rate of 5 °C min^{-1}. Solid-state ^1H and ^2H NMR spectra were measured by a solid echo pulse sequence $\pi/2_x-\tau-\pi/2_y$ using a Bruker DSX 300 spectrometer; the values for the $\pi/2$ pulse width and τ were 1.2 and 10 μs for ^1H NMR and 2.5 and 13 μs for ^2H NMR. The ^2H NMR spectra were measured under a constant pressure of 0.1 MPa of CO_2 (only for **1a′**) and under 0.1 MPa of N_2 (for all others) for all temperatures. For measurement of **1a′** under CO_2, a gas-handling system was constructed for the NMR probe. The sample was degassed by a rotary pump and then 0.1 MPa of CO_2 was introduced through the gas-handling system.

Acknowledgment. This work was financially supported by the Ministry of Education, Culture, Sports, Science and Technology, Japan (Nos. 18750051, 18033043 (S.T.), and 18350002 (S.T.)) and as a PRESTO (Precursory Research for Embryonic Science and Technology) project from the Japan Science and Technology Agency.

Note Added after ASAP Publication. This article published ASAP on February 25, 2010 with an incorrect version of Figure 2 and the caption. The correct version posted March 17, 2010.

Supporting Information Available: Additional X-ray structures of CO_2-included crystal hosts, DSC spectral data of CO_2 adsorption of the crystal hosts, thermal parameters calculated from that chart, and additional solid-state NMR spectra of CO_2-included crystal hosts. This material is available free of charge via the Internet at http://pubs.acs.org.

JA9091598

(28) Takamizawa, S.; Hiroki, T.; Nakata, E.; Mochizuki, K.; Mori, W. *Chem. Lett.* **2002**, *31*, 1208.

(29) Takamizawa, S.; Akatsuka, T.; Miyake, R. *CrystEngComm* **2010**, *12*, 82.